The dynamics of charge transfer with and without a barrier: A very simplified model of cyclic voltammetry

Wenjun Ouyang, and Joseph E. Subotnik

Citation: The Journal of Chemical Physics **146**, 174103 (2017); doi: 10.1063/1.4979620
View online: http://dx.doi.org/10.1063/1.4979620
View Table of Contents: http://aip.scitation.org/toc/jcp/146/17
Published by the American Institute of Physics

The dynamics of charge transfer with and without a barrier: A very simplified model of cyclic voltammetry

Wenjun Ouyang and Joseph E. Subotnik[a)]
Department of Chemistry, University of Pennsylvania, Philadelphia, Pennsylvanian 19104, USA

(Received 20 December 2016; accepted 21 March 2017; published online 1 May 2017)

Using the Anderson-Holstein model, we investigate charge transfer dynamics between a molecule and a metal surface for two extreme cases. (i) With a large barrier, we show that the dynamics follow a single exponential decay as expected; (ii) without any barrier, we show that the dynamics are more complicated. On the one hand, if the metal-molecule coupling is small, single exponential dynamics persist. On the other hand, when the coupling between the metal and the molecule is large, the dynamics follow a biexponential decay. We analyze the dynamics using the Smoluchowski equation, develop a simple model, and explore the consequences of biexponential dynamics for a hypothetical cyclic voltammetry experiment. *Published by AIP Publishing.* [http://dx.doi.org/10.1063/1.4979620]

I. INTRODUCTION

Charge transfer between a metal and a surface-tethered molecule is fundamentally different from the typical inter- or intra-molecular charge transfer prevalent in photoexcited dynamics because a metal consists of a continuum of states (rather than a sum of discrete states). The standard model for studying charge transfer between a discrete state and a manifold of states is the Anderson-Holstein (AH) model.[1,2] For instance, the AH model has been used to study inelastic electron tunneling spectra,[3–6] the ultrafast electron transfer reaction at a dye-semiconductor interface,[7–10] and hysteresis at very low temperatures (including the effects of tunneling).[11–16] This list is not exhaustive, e.g., see Ref. 5 for a review of the theory of electron-phonon couplings in the context of molecular conduction (which routinely uses the Anderson-Holstein model).

Over the last two decades, a few research groups have explored the AH model in the high temperature limit, where nuclear vibrations can be considered classical (and we need not worry about nuclear quantization). In such a limit, the AH model lends itself to several quasi-classical interpretations,[17–27] all of which can and should be compared with classical Marcus theory[22] at least in principle:

- Shenvi *et al.*[23] developed the independent electron surface hopping algorithm which explicitly discretizes the metal continuum and runs fewest-switches surface hopping with a large number of electronic states under the assumption of noninteracting electrons.
- Schmickler *et al.* proposed running heuristic nuclear trajectories on mean-field surfaces followed by collapsing events to diabatic PESs.[28]
- Mohr *et al.*[24] calculated electron transfer rates effectively by performing perturbation theory in the electron-phonon couplings and evaluating short time dynamics; these methods gave insight into both adiabatic electron transfer and nonadiabatic electron transfer but ignored long-time feedback on the solvent nuclear motion.
- Kuznetsov *et al.*[25] explicitly discretized the continuum of electronic states and suggested running stochastic Monte Carlo simulations to simulate electron transfer, whereby trajectories used Landau-Zener rates at crossing points to determine when to switch diabatic Gibbs free energy surfaces. Preliminary results recapitulated the correct physics for the limits of weak and strong electron coupling; extensions to non-quadratic surfaces have not yet been investigated.
- Inspired by the work of Schmickler *et al.*, Mishra and Waldeck[26,27] not long ago calculated approximate rates for electron transfer from molecule to metal using two methods: one labeled a "density of state" model (which averaged Fermi's golden rule rates and treated nuclear motion only implicitly) and one labeled a "potential energy curve" model, whereby one considered an explicit nuclear reactions coordinate and used a variation of Landau-Zener transition state theory to calculate electron transfer rates by summing over a continuum of states.

Beyond the approaches above, over the last few years, our research group has chosen to work with two more dynamic models, neither of which requires discretizing an electronic continuum. On the one hand, in the limit of small molecule-metal couplings, one can invoke perturbation theory to derive a classical master equation (CME),[19] which might be the simplest and most intuitive approach for simulating electron transfer dynamics. On the other hand, in the limit of large molecule-metal couplings, one can derive a model of electronic friction that reflects a molecule exchanging electrons rapidly and frequently with the metal (resulting in electronic friction plus a random force).[17,20,29] These two approaches can be bridged using a broadened classical master equation (BCME),[21] but for the purposes of the present article, we will not consider broadening (and the CME suffices).

a)Electronic mail: subotnik@sas.upenn.edu

Now, to measure the effects of charge transfer at a metal surface, the most basic technique is cyclic voltammetry (CV).[30] In a typical electrochemical experiment, one coats an electrode with a selective, microporous material, and a CV experiment measures the current through ions at metal interfaces at different driving forces. To correctly interpret a CV curve, a key element is the ramping rate, i.e., the rate at which the driving force changes (and one measures the dynamical response of the current). If we consider the dynamics of electrochemical charge transfer within the context of standard Marcus theory, at some points in a CV curve the driving force will be small (with a large barrier, corresponding to the normal regime); for other points in a CV curve, the driving force will be larger (without any barrier, corresponding either to the barrierless regime or to the "inverted" regime).[31] See Fig. 1 for a schematic view of the different regimes. The ramping rate represents how fast we switch between these two extreme limits. The fact that CV curves depend on the ramping rate suggests that a complete theoretical model must explain both (i) steady-state charge transfer between the molecule and the electrode at any driving force (i.e., the analogues of the normal, barrierless, and inverted Marcus regimes) and (ii) the non-equilibrium effects that arise for charge transfer because the ramping rate is not infinitesimally slow, such that nuclei are not fully relaxed at every driving force. The latter effect results in hysteresis in most CV curves.

The goal of the present paper is to investigate these exact charge transfer dynamics (for a large range of parameter space). We will show several interesting features below. First, regarding the rate of charge transfer, on one hand, we will show that if the metal-molecule coupling is small, charge transfer dynamics always follow single exponential dynamics. However, on the other hand, when the coupling between the metal and the molecule is large and there is no barrier, the dynamics follow a biexponential decay. In other words, there are two competing time scales, and standard chemical rate theory is not easily applicable. Second, regarding non-equilibrium effects, we will show that non-equilibrium effects arise when the ramping rate is large.

Finally, before concluding this introduction, we mention that, in the limit of a very small ramping rate and a large reservoir of electrons, a CV experiment recovers a simple, universal current vs. overpotential (voltage) plot, which is known as a Tafel plot.[32,33] To construct a model of a Tafel plot with trajectories, one requires two electronic baths so as to enforce a potential difference at steady state. In the present paper, we focus exclusively on the case of a single electronic bath and investigate transient charge transfer dynamics. In the future, it will be interesting to explore whether any effects of biexponential decay dynamics can be observed in current-voltage plots.

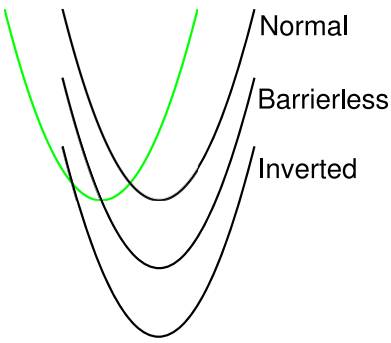

FIG. 1. A schematic picture of different regimes for charge transfer. The donor state is colored green, and the possible acceptor states are colored black.

We organize the paper as follows. In Section II, we define the Hamiltonian and review the CME and corresponding Smoluchowski master equation. In Section III, we present and analyze results from the CME and Smoluchowski master equation simulations; furthermore, a simple biexponential model is proposed and investigated to study barrierless, large-coupling dynamics. In Section IV, we discuss the implications of our results for cyclic voltammetry. We conclude in Section V.

II. THEORY

A. The Hamiltonian

Without any external friction, the Hamiltonian of a generalized AH model can be written as follows:

$$H = H_s + H_b + H_c, \tag{1a}$$

$$H_s = E(x)d^\dagger d + V_0(x) + \frac{p^2}{2m}, \tag{1b}$$

$$H_b = \sum_k (\varepsilon - \mu) c_k^\dagger c_k, \tag{1c}$$

$$H_c = \sum_k \tilde{W}_k \left(c_k^\dagger d + d^\dagger c_k \right). \tag{1d}$$

d ($d^\dagger$) is the creation (annihilation) operator for an electronic impurity level and c_k ($c_k^\dagger$) is the creation (annihilation) operator for a manifold of electronic states modeling the metal surface. μ is the chemical potential of the metal surface. The two diabatic states are modeled as two shifted harmonic oscillators

$$V_0(x) = \frac{1}{2} m\omega^2 \left(x + \frac{g}{2} \right)^2, \tag{2a}$$

$$V_1(x) \equiv V_0(x) + E(x) = \frac{1}{2} m\omega^2 \left(x - \frac{g}{2} \right)^2 - \Delta G^0. \tag{2b}$$

ΔG^0 is the bias between two states. The coupling between the two states and the metal surface is characterized as a hybridization function $\Gamma/\hbar$, where $\Gamma = \Gamma(\varepsilon) \equiv 2\pi \sum_k \left| \tilde{W}_k \right|^2 \delta(\varepsilon_k - \varepsilon)$ under the wide band approximation.

B. Surface hopping/classical master equation

In the limit of small Γ, one can perform Redfield theory and find a simple set classical master equation that governs the dynamics of the AH Hamiltonian. In a CME simulation, the nuclei are propagated on one of the two electronic states, and the charge transfer is modeled as surface hopping between the two electronic states. Denoting the probability density for the electronic impurity level to be unoccupied (occupied) as P_0 (P_1), the CME can be written as[19]

$$\frac{\partial P_0(x,p,t)}{\partial t} = \frac{\partial V_0(x,p)}{\partial x} \frac{\partial P_0(x,p,t)}{\partial p} - \frac{p}{m} \frac{\partial P_0(x,p,t)}{\partial x} - \zeta_{0\to 1} P_0(x,p,t) + \zeta_{1\to 0} P_1(x,p,t), \tag{3a}$$

$$\frac{\partial P_1(x,p,t)}{\partial t} = \frac{\partial V_1(x,p)}{\partial x}\frac{\partial P_1(x,p,t)}{\partial p} - \frac{p}{m}\frac{\partial P_1(x,p,t)}{\partial x} + \zeta_{0\to1}P_0(x,p,t) - \zeta_{1\to0}P_1(x,p,t). \quad (3b)$$

The transfer probabilities ζ are defined as

$$\zeta_{0\to1} = \frac{\Gamma}{\hbar}f_\mu(V_1(x) - V_0(x)), \quad (4a)$$

$$\zeta_{1\to0} = \frac{\Gamma}{\hbar}f_{-\mu}(V_0(x) - V_1(x)). \quad (4b)$$

Here $f_\mu(\varepsilon)$ is the Fermi function

$$f_\mu(\varepsilon) = \frac{1}{1+e^{\beta(\varepsilon-\mu)}}. \quad (5)$$

To investigate the charge transfer rate, one keeps the chemical potential μ fixed and looks at the population transition in time. In Section IV, we will simulate a CV-like experiment by changing μ continuously and investigating the electronic population as a function of μ.

C. Smoluchowski master equation

In the present paper, we are interested in coupled nuclear-electron dynamics through the AH Hamiltonian *in the presence of external nuclear friction*. To that end, we will introduce external friction through Langevin dynamics with the usual equation of motion. For example, on one surface, we write

$$m\ddot{x} = -\gamma\dot{x} - \frac{dU(x)}{dx} + \sqrt{2\gamma k_b T}R(t). \quad (6)$$

$U(x)$ is the potential energy and $R(t)$ is the Markovian random variable from a standard normal distribution. In the limit of large γ, the left hand side of Eq. (6) can be neglected, and the corresponding Fokker-Planck (FP) equation for the distribution function in position is known as Smoluchowski equation ($W = W(x,t)$),

$$\frac{\partial W}{\partial t} = \frac{1}{\gamma}\left(\frac{\partial}{\partial x}\frac{dU(x)}{dx} + k_b T\frac{\partial^2}{\partial x^2}\right)W \equiv \mathcal{L}_{FP}W. \quad (7)$$

Now, for the case of the classical master equation in Eq. (3), with external friction the corresponding FP equations become

$$\frac{\partial P_0(x,p,t)}{\partial t} = \frac{\partial V_0(x,p)}{\partial x}\frac{\partial P_0(x,p,t)}{\partial p} - \frac{p}{m}\frac{\partial P_0(x,p,t)}{\partial x} + \frac{\gamma}{m}\frac{\partial}{\partial p}(pP_0(x,p,t)) + \gamma k_b T\frac{\partial^2 P_0(x,p,t)}{\partial p^2} - \zeta_{0\to1}P_0(x,p,t) + \zeta_{1\to0}P_1(x,p,t), \quad (8a)$$

$$\frac{\partial P_1(x,p,t)}{\partial t} = \frac{\partial V_1(x,p)}{\partial x}\frac{\partial P_1(x,p,t)}{\partial p} - \frac{p}{m}\frac{\partial P_1(x,p,t)}{\partial x} + \frac{\gamma}{m}\frac{\partial}{\partial p}(pP_1(x,p,t)) + \gamma k_b T\frac{\partial^2 P_1(x,p,t)}{\partial p^2} + \zeta_{0\to1}P_0(x,p,t) - \zeta_{1\to0}P_1(x,p,t). \quad (8b)$$

Furthermore, in the case of large external friction, the Smoluchowski equation is

$$\frac{\partial W_0}{\partial t} = \mathcal{L}^{(0)}_{FP}W_0 - \zeta_{0\to1}W_0 + \zeta_{1\to0}W_1, \quad (9a)$$

$$\frac{\partial W_1}{\partial t} = \mathcal{L}^{(1)}_{FP}W_1 + \zeta_{0\to1}W_0 - \zeta_{1\to0}W_1. \quad (9b)$$

We will abbreviate Eq. (9) as a "SME" (for Smoluchowski master equation). Note that W_i in Eq. (9) is different from P_i in Eq. (3) in that the momentum dependence is absent, which simplifies the analysis dramatically.

Consider now the SME operator $\mathcal{M}$,

$$\mathcal{M} \equiv \begin{pmatrix} \mathcal{L}^{(0)}_{FP} - \zeta_{0\to1} & \zeta_{1\to0} \\ \zeta_{0\to1} & \mathcal{L}^{(1)}_{FP} - \zeta_{1\to0} \end{pmatrix}. \quad (10)$$

The SME operator is non-Hermitian given that $\mathcal{L}^{(i)}_{FP}$ is non-Hermitian and the off-diagonal blocks are asymmetric, which makes diagonalization very unstable. Let us now show that we can transform the SME operator into a Hermitian matrix, where diagonalization is stable.

To proceed, note that there is a well-known technique[34] to transform the non-Hermitian Fokker-Planck operator $\mathcal{L}_{FP}$ into a Hermitian matrix $\mathcal{L}$,

$$\mathcal{L}^{(i)} = e^{\Phi_i/2}\mathcal{L}^{(i)}_{FP}e^{-\Phi_i/2}, \ (i = 0, 1), \quad (11)$$

$$\Phi_i \equiv \beta V_i(x) + C_i, \ (i = 0, 1). \quad (12)$$

Here C is a constant typically chosen as 0 and can be neglected for calculations on a single surface. This constant becomes crucially important, however, if we apply such a similarity transformation to the SME operator $\mathcal{M}$ for two surfaces. In such a case, we define a transformation matrix U as

$$U = \begin{pmatrix} e^{\beta(V_0(x)+\mu)/2} & 0 \\ 0 & e^{\beta V_1(x)/2} \end{pmatrix}. \quad (13)$$

Note here that, in the upper left, we write $V_0(x) + \mu$ (instead of $V_0(x)$). The SME operator after transformation becomes

$$\begin{aligned}\tilde{\mathcal{M}} &\equiv U\mathcal{M}U^{-1} \\ &= \begin{pmatrix} \mathcal{L}^{(0)} - \zeta_{0\to1} & \zeta_{1\to0}e^{\beta\Delta V/2} \\ \zeta_{0\to1}e^{-\beta\Delta V/2} & \mathcal{L}^{(1)} - \zeta_{1\to0} \end{pmatrix} \\ &= \begin{pmatrix} \mathcal{L}^{(0)} - \zeta_{0\to1} & \frac{\Gamma}{2\hbar}\mathrm{sech}\left(\frac{\beta\Delta V}{2}\right) \\ \frac{\Gamma}{2\hbar}\mathrm{sech}\left(\frac{-\beta\Delta V}{2}\right) & \mathcal{L}^{(1)} - \zeta_{1\to0} \end{pmatrix}. \end{aligned} \quad (14)$$

ΔV is defined as

$$\Delta V \equiv V_0(x) + \mu - V_1(x). \quad (15)$$

Given that the sech function is an even function, the operator $\tilde{\mathcal{M}}$ is a Hermitian operator. Henceforward, we will work with $\tilde{\mathcal{M}}$. Note that a similarity transformation alters eigenvectors but all eigenvalues are unchanged. In Section III we will diagonalize $\tilde{\mathcal{M}}$ to analyze the dynamics.

Before presenting any results, we note that the present analysis is very much the spirit of Ref. 35, where Cao and Jung numerically diagonalized the Fokker-Planck operator for a two-state Hamiltonian (through the quantum-classical Liouville equation[36–45]) in order to investigate electron transfer kinetics in the over-damped limit. The authors then compared their results to those of Zusman[46] or, equivalently, Straub and Berne,[47] and Rips and Jortner.[48] In comparison with Ref. 35, note that the present work treats a continuum of states (rather than the usual two-state dynamics), and in such a case, there is no Zusman-like analytic theory or rate expression for the rate in the over-damped regime. It is important to remember

that, unlike the case of two-state spin-boson dynamics, for the present Anderson-Holstein model, there is no turnover in the electron transfer rate in the inverted regime; furthermore, the notion of electronic friction makes sense only with a continuum of states (not with a two-state model) such that one can almost consider many reactions adiabatic even with a small diabatic coupling.[22,49] That being said, whereas Cao and Jung used the quantum-classical Liouville equation to identify different regimes of electron transfer as a function of dissipation strength, below we will effectively show that different regimes can also be identified through Fokker-Planck CME dynamics.

III. RESULTS

For the system defined in Eq. (2), we choose the following parameters (in atomic units): $m = 2000$, $\omega = 0.0002$, and $g = 21.795$. The reorganization energy is $E_r = 20k_bT$, and the temperature is 300 K. The nuclear friction is $\gamma = 4$ a.u., which is 5 times of friction for a damped harmonic oscillator ($2m\omega$). The chemical potential is $\mu = 0$.

A. SME and CME

To begin our analysis, we will first demonstrate that our propagation of the SME in Eq. (14) on a one-dimensional grid reproduces our CME results with trajectories. Fig. 2 shows the electronic population (P_0) as a function of time for the cases of different biases ($\Delta G^0 = 0k_bT$ and $\Delta G^0 = 20k_bT$) and different coupling strengths ($\Gamma/\hbar = 10^{-5}$ and 4×10^{-4} a.u.). The initial condition is the equilibrium Gaussian distribution on state 0 for all cases. The agreement between the results from the SME calculation and the CME simulation is excellent. We also fit the CME results to a single exponential decay,

$$P = c_1 + c_2 e^{-c_3 t}, \tag{16}$$

where c_i are the parameters to be fit. The single exponential fits agree well with the CME results except for Fig. 2(d). In Fig. 2(d), we successfully fit the CME result to a biexponential instead,

$$P = c_1 + c_2 e^{-c_3 t} + c_4 e^{-c_5 t}. \tag{17}$$

Here we observe biexponential decay in the barrierless regime when the coupling is large but single exponential decay when the coupling is small. We may conclude that, in the barrierless case, if Γ is small enough and can be considered as a small perturbation to the system, the system will always maintain local equilibrium of velocities and positions, and there is only one rate of decay (i.e., the rate of escape into the product well). By contrast, if the coupling is larger, local equilibrium is violated and there is no unique rate.

B. Eigenvalues of the SME operator

The biexponential decay in Fig. 2 indicates that there are two distinct time scales involved. In order to assess these two time scales, we diagonalize the SME operator: every eigenvalue is the decay rate for a corresponding right eigenstate,

$$\mathcal{L}\phi_n = -\lambda_n \phi_n. \tag{18}$$

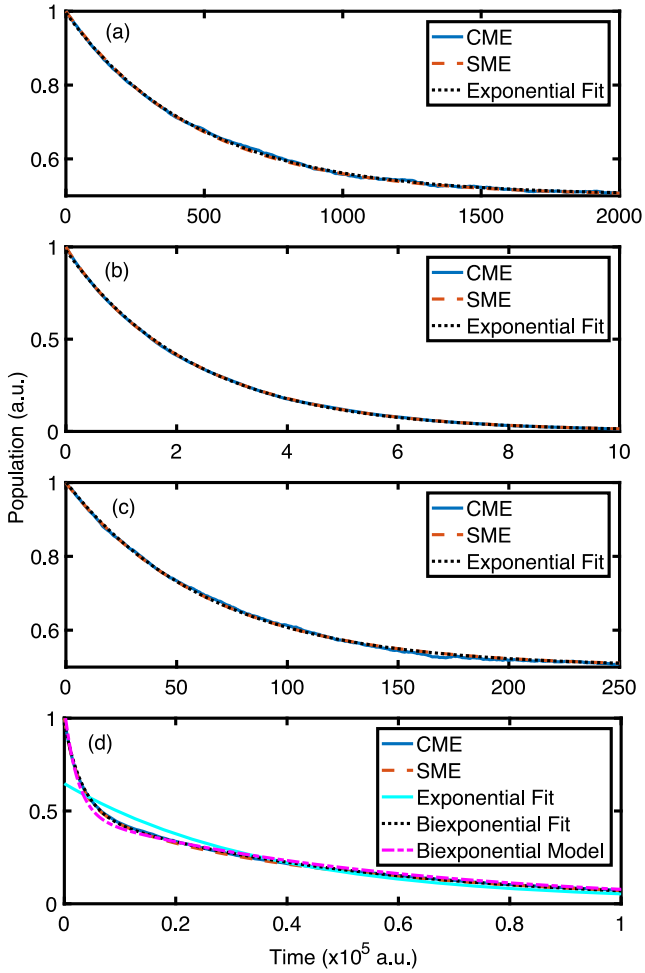

FIG. 2. The electronic population (P_0) as a function of time. The common parameters for the system are listed in the beginning of Section III. (a) $\Delta G^0 = 0k_bT$, $\Gamma/\hbar = 10^{-5}$ a.u.; (b) $\Delta G^0 = 0k_bT$, $\Gamma/\hbar = 4 \times 10^{-4}$ a.u.; (c) $\Delta G^0 = 20k_bT$, $\Gamma/\hbar = 10^{-5}$ a.u.; (d) $\Delta G^0 = 20k_bT$, $\Gamma/\hbar = 4 \times 10^{-4}$ a.u. The SME calculation agrees well with the CME simulation. The single exponential fit works well for all but the case of a barrierless regime with large coupling; in such a case a biexponential fit works well. The biexponential fit is $0.004 + 0.49 \times \exp(-2 \times 10^{-5} t) + 0.48 \times \exp(-3.1 \times 10^{-4} t)$.

Note that the minus sign on the right hand side makes λ_n positive definite. Fig. 3 shows the eigenvalues as a function of bias for the cases of different coupling strength. The ground eigenvector always has an eigenvalue of zero denoting the equilibrium (stationary) state, and thus we focus on the excited eigenvectors. When the coupling strength is small (Fig. 3(a)), the first excited "diabatic" eigenvalue increases from the Marcus rate at small bias to $\Gamma/\hbar$ at large bias, which is what we have expected (when the bias is large the system converges to a two-level system). However, when the coupling strength is large (Fig. 3(b)), the phenomenon is qualitatively different. (i) The first excited "diabatic" eigenvalue, which is highlighted by cross markers and denoted as $\tilde{V}_1$, does not converge to $\Gamma/\hbar$ in large bias but rather keeps increasing and crosses the value of $\Gamma/\hbar$; (ii) instead, in this case, there is a higher excited "diabatic" eigenvalue, which is highlighted by circle markers and denoted as $\tilde{V}_2$, which decreases to $\Gamma/\hbar$ from above.

The results here are very different from Ref. 35 in the inverted regime. While the charge transfer rate should decrease in the inverted regime according to Marcus theory, which is

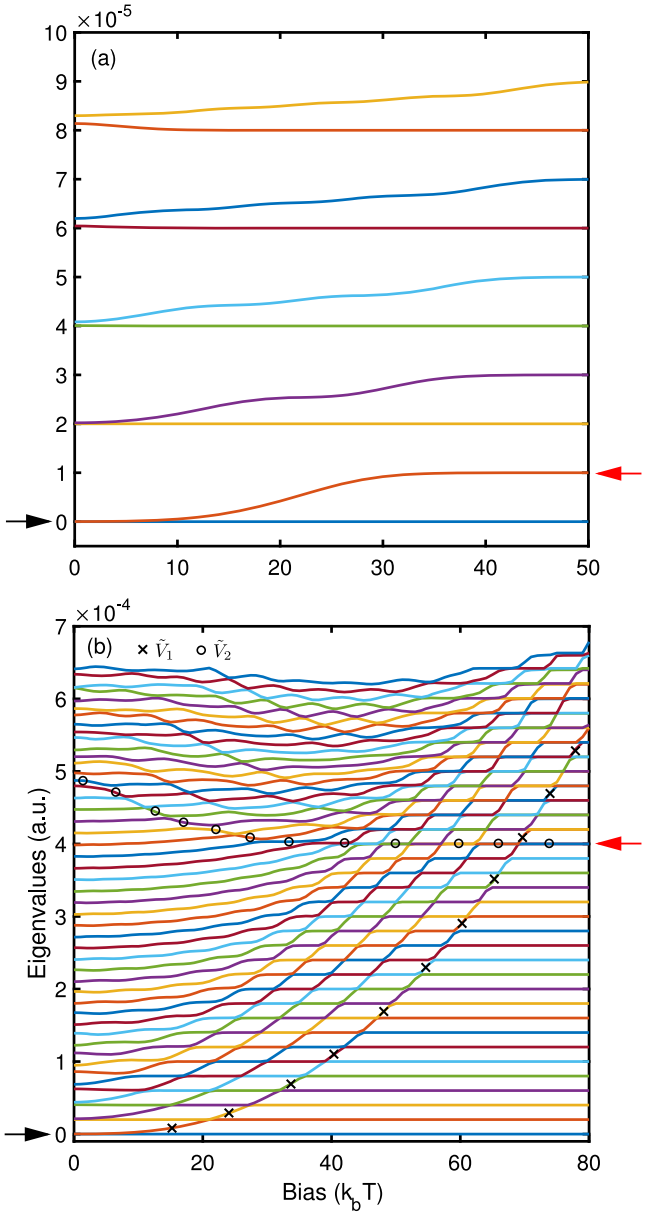

FIG. 3. Eigenvalues of an SME operator as a function of bias. (a) $\Gamma/\hbar = 10^{-5}$ a.u., and the first ten states are plotted; (b) $\Gamma/\hbar = 4\times10^{-4}$ a.u., and the first 50 states are plotted. The Marcus rate in the small bias limit and the rate $\Gamma/\hbar$ in the large bias limits are highlighted by the black and red arrows, respectively. For small coupling, the first excited state increases to $\Gamma/\hbar$ at large bias. But for large coupling, the first excited "diabatic" eigenvalue ($\tilde{V}_1$, black cross) is monotonically increasing and a higher excited eigenvalue ($\tilde{V}_2$, black circle) decreases and plateaus at $\Gamma/\hbar$.

the case in Ref. 35, the rate in Fig. 3 saturates in the large bias due to the presence of metal surface.

C. A biexponential model

The unusual phenomenon in Fig. 3(b) indicates that there are two time scales involved and, in order to build a simple biexponential model, we can take the eigenvalues of $\tilde{V}_1$ and $\tilde{V}_2$ as those two rates,

$$P = c_1 + c_2 e^{-r_1 t} + c_3 e^{-r_2 t}. \tag{19}$$

Here, r_i should be extracted from Fig. 3(b) and c_i are the parameters to be fit to the CME result. The two rates extracted from Fig. 3(b) at $\Delta G^0 = 20k_bT$ are 1.76×10^{-5} and 4.2×10^{-4}. Comparing with the biexponential fit to the CME simulation (Fig. 2(d): 2×10^{-5} and 3.1×10^{-4}), we slightly overestimate the fast rate but underestimate the slow rate. Fig. 2(d) also shows the electronic population as a function of time using our biexponential model. The discrepancy between our biexponential model and CME result is not significant despite the difference in the two rates.

D. Projection of initial condition

From Figs. 2(d) and 3(b), we may conclude that the three eigenvalues discussed above in Section III C characterize the overall dynamics in a semi-quantitative fashion. To characterize exactly how quantitative is our biexponential model, we will project our initial conditions onto the full set of eigenvectors and define the absolute value of each coefficient as the weight of each eigenstate. These weights offer a simple tool for analysis.

When the bias is $0k_bT$, we find that the lowest and the first excited eigenvector—which together predict a single exponential decay—make up 90% of the total sum of the weights. However, when the bias is $20k_bT$, we find that the ground eigenvector, $\tilde{V}_1$, and $\tilde{V}_2$—which together give the biexponential model in Section III C—make up only 24% of the total weights. This small weight explains the discrepancy in Fig. 2(d) between the biexponential model and the biexponential fit, as there are clearly more than three relevant eigenvectors.

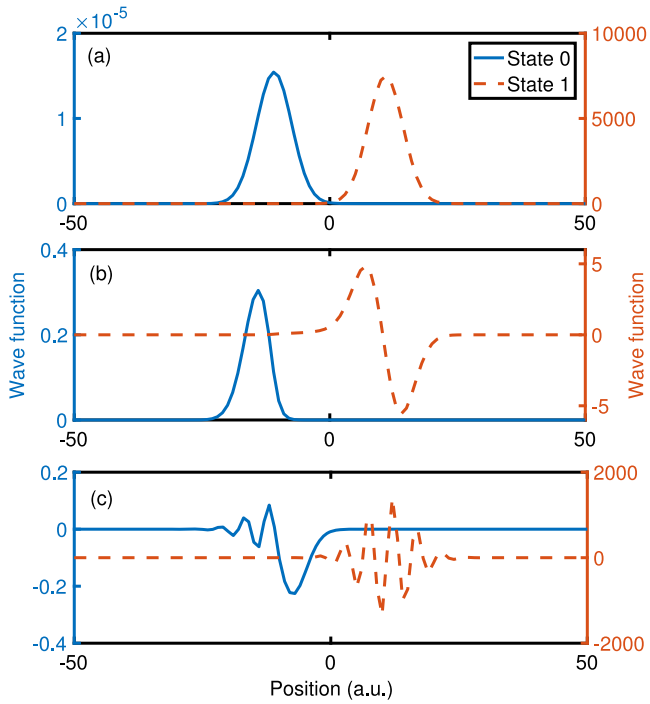

FIG. 4. The three right eigenvectors of the SME operator comprising our biexponential model with a bias of $20k_bT$. The vectors themselves are not normalized after the inverse transformation (Eq. (13)) back to real space. The left y-axis is associated with the state 0 (all colored blue), and the right y-axis is associated with the state 1 (all colored red). Recall that state 0 corresponds to the uncharged molecule and state 1 corresponds to the charged molecule. (a) The ground eigenvector; (b) the first excited eigenvector; (c) the 31st eigenvector. The large proportion of the populations between the two electronic states comes from the large bias. The structures of the eigenvectors are obscure which is consistent with the fact that the initial condition is mixed significantly with many other eigenvectors.

To give more intuition for this approach, for a bias of $20k_bT$, we show the three relevant right eigenvectors in Fig. 4. Note that most of the electronic population from these eigenvectors resides on state 1 (rather than state 0) because of the large bias. Furthermore, the lowest and first excited eigenvectors are perhaps intuitive: they appear to be the ground and first excited states of the harmonic oscillator on state 1. That being said, it becomes very difficult to interpret any clear physical meaning from the 31st state, i.e., the lowest lying state that converges to $\Gamma/\hbar$ at large bias.

IV. DISCUSSION: A CONNECTION TO CYCLIC VOLTAMMETRY

To connect the results above with a cyclic voltammetry experiment, we will now perform a Gedanken experiment. With a ramping rate (to be specified later), we will move ΔG^0 up and down so that states 0 and 1 switch between the least and most stable. We consider the electronic population (P_0) on the impurity as a function of time, both for the case of small and large coupling (Γ).

Fig. 5 shows the electronic population as a function of bias in the case of small coupling ($\Gamma = 10^{-5}$ a.u.). Besides the raw CME simulation data, we also plot results from a simple integration of

$$\frac{d}{dt}\begin{pmatrix} P_0 \\ P_1 \end{pmatrix} = \begin{pmatrix} -k_{0\to1}(t) & k_{1\to0}(t) \\ k_{0\to1}(t) & -k_{1\to0}(t) \end{pmatrix}\begin{pmatrix} P_0 \\ P_1 \end{pmatrix}. \tag{20}$$

k in Eq. (20) is the electron transfer rate according to Marcus theory,

$$k_{1\to0}(t) = \int_{-\infty}^{\infty} d\varepsilon \frac{\Gamma(\varepsilon)}{\hbar}\left(1 - f_\mu(\varepsilon)\right)\frac{e^{-(E_r-\Delta G^0(t)+\varepsilon)^2/4E_rk_bT}}{\sqrt{4\pi E_r k_b T}}, \tag{21a}$$

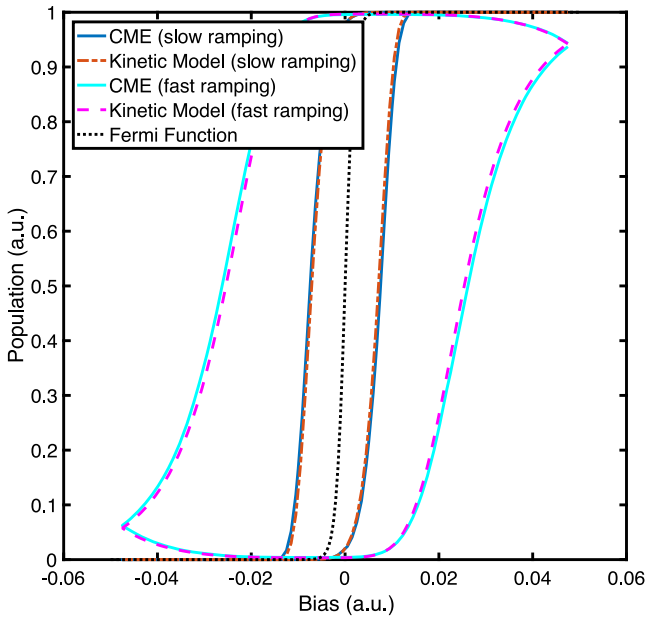

FIG. 5. The electronic population (P_0) as a function of bias. The coupling is $\Gamma/\hbar = 10^{-5}$ a.u. The slow and fast ramping rates are 10^{-9} a.u. and 10^{-7} a.u., respectively. The bias range is [−0.475, 0.475] a.u. For the case of fast ramping, 10 iterations of ramping are simulated to converge the result. Our kinetic model (Eqs. (20) and (21)) agrees well with the CME results.

$$k_{0\to1}(t) = \int_{-\infty}^{\infty} d\varepsilon \frac{\Gamma(\varepsilon)}{\hbar} f_\mu(\varepsilon)\frac{e^{-(E_r+\Delta G^0(t)-\varepsilon)^2/4E_rk_bT}}{\sqrt{4\pi E_r k_b T}}. \tag{21b}$$

For both slow and fast ramping rates, Eqs. (20) and (22) agree well with the CME simulation. This agreement suggests that, when the diabatic coupling is small enough, the local equilibrium of position and velocities is largely maintained for each state, such that the Marcus theory is still applicable.

Now, in the case of large coupling ($\Gamma = 4 \times 10^{-4}$ a.u.), even though Marcus theory (Eqs. (20) and (21)) is expected to fail, we would still like an analytic model (in the spirit of Eq. (21)) to compare against our CME data. Furthermore, unfortunately, we showed above that no single exponential model is possible in the barrierless regime. With this limitation in mind, we will compare our CME data versus a crude model for the electron transfer using a discontinuous rate. In particular, with reference to the eigenvalues in Fig. 3, we stipulate that when there is a barrier between two states (corresponding to bias within $\pm 20k_bT$ for this particular problem), we use the first excited "diabatic" eigenvalue $\tilde{V}_1$; when there is no barrier between two states (corresponding to bias outside $\pm 20k_bT$ for this particular problem), we use the lowest "diabatic" eigenvalue that converges to $\Gamma/\hbar$ in large bias $\tilde{V}_2$. See Fig. 3(b) for a means to visualize $\tilde{V}_1$ and $\tilde{V}_2$,

$$k_{spline}(t) = \begin{cases} \tilde{V}_1, & |\Delta G^0(t)| \le E_r \\ \tilde{V}_2, & |\Delta G^0(t)| > E_r \end{cases}. \tag{22}$$

With this model, for both fast and slow ramping rates, Fig. 6 plots the electronic population as a function of bias for the first cycle up and down. According to Fig. 6, the model calculation roughly agrees with a CME simulation. The

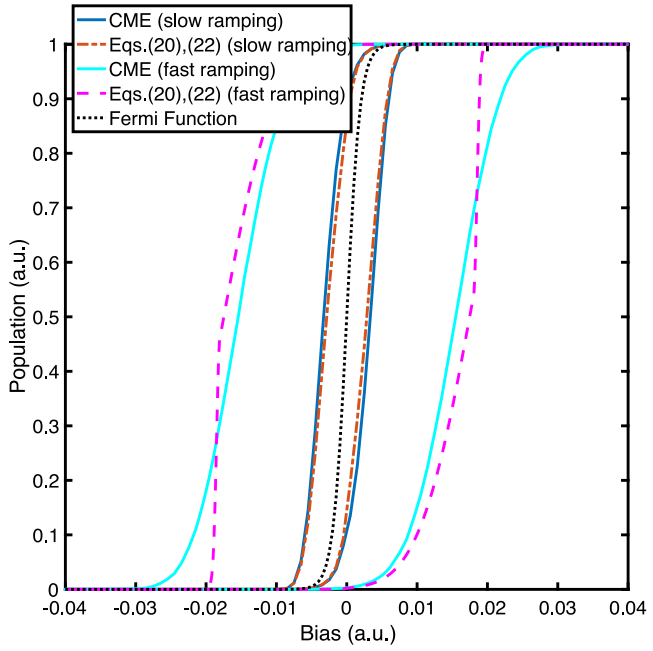

FIG. 6. The electronic population (P_0) as a function of bias. The coupling is $\Gamma/\hbar = 4 \times 10^{-4}$ a.u. The slow and fast ramping rates are 10^{-9} a.u. and 10^{-7} a.u., respectively. The bias range is [−0.475, 0.475] a.u. Eqs. (20) and (22) use the eigenvalues in Fig. 3 as the electron transfer rates. See text for more detail. The large errors for the kinetic model (Eqs. (20) and (22)) in the case of a fast ramping rate indicate that one cannot use a single rate to reproduce the correct dynamics.

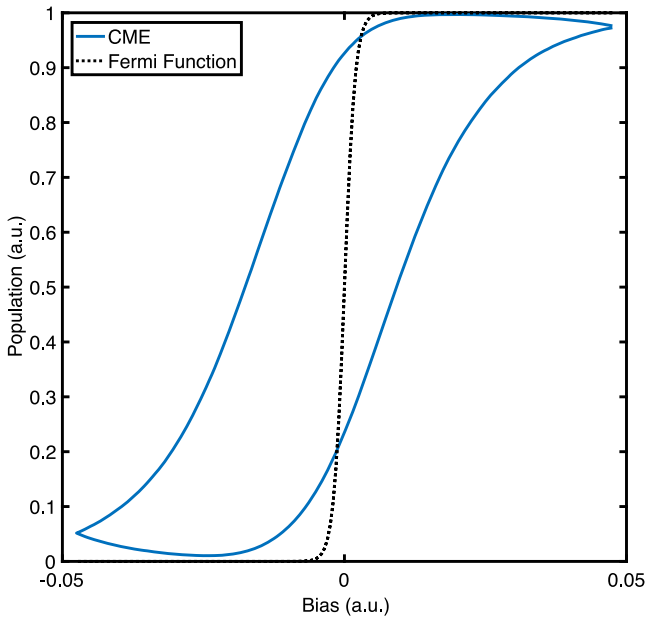

FIG. 7. The electronic population (P_0) as a function of bias. The coupling is $\Gamma/\hbar = 4 \times 10^{-4}$ a.u. The ramping rate is 5×10^{-6} a.u. 10 iterations of ramping are simulated to converge the result. The Fermi function is not within the hysteresis as in Figs. 5 and 6, which demonstrates clear non-equilibrium effects: the nuclear relaxation time is comparable with the ramping rate such that the nuclei do no remain equilibrated in time.

differences between the CME results and the kinetic model calculations imply that our crude model is simply too simplistic: one cannot use a single rate to reproduce the true CME dynamics. Recall Fig. 2. While non-equilibrium effects from the finite ramping rate might be another reason that we see the disagreement in Fig. 6 (especially for the case of large ramping rate), we believe that the failures in Fig. 6 should be traced largely to difference at equilibrium, i.e., the incapability of the simple model. For instance, note that the CME curve in Fig. 6 ramps between 0 and 1, indicating that the electronic population is able to relax before the bias sweeping reverses the direction.

Finally, if we wish to expose the most egregious non-equilibrium effects, Fig. 7 plots the electronic population as a function of bias with an even larger ramping rate of 5×10^{-6} a.u. When compared with the Fermi function, unlike Figs. 5 and 6, we now see that the Fermi function is not fully contained within the hysteresis loop, which implies that dynamical charge transfer can occur even before such charge transfer is stabilized by equilibrium conditions. This phenomenon cannot be explained under the assumption of local equilibrium but rather must be caused exclusively by non-equilibrium effects. Given that many rate theories assumes local equilibrium, it will be difficult (but very interesting) to develop a kinetic model that can reproduce such non-equilibrium effects.[50]

V. CONCLUSION

We have analyzed biexponential dynamics of charge transfer in the high barrier and barrierless regime using CME and SME dynamics. The SME calculations agree with the CME simulations in all cases and an exponential/biexponential fit works very well in practice; biexponential dynamics are manifested only when the coupling is large so that local equilibrium is broken. To understand these biexponential dynamics, we have attempted to map the empirical decay rates to the eigenvalues of the SME operator. Unfortunately, this mapping becomes difficult because many (i.e., more than 2) eigenvectors participate. Fig. 3 shows two different scenarios for how SME eigenvalues change with driving force, and we see analogies to avoided crossings in molecular systems.

Finally, we have studied the effect of these biexponential dynamics on a hypothetical cyclic voltammetry curve (looking at the electronic population instead of the current) shown in Figs. 5 and 6. Perhaps not surprisingly, we find that a simple kinetic model is appropriate when the coupling is small (so that all dynamics are exponential). For larger couplings, a practical switching model for the rate (as in Eq. (22)) is only moderately successful; see Fig. 6. It remains an open question whether or not one can extract a better, more accurate kinetic model for a system like this with biexponential decay. A kinetic model would appear almost impossible for the case of large couplings and large ramping rates, as in Fig. 7, where local equilibrium appears to be almost nonexistent and charge transfer can occur ahead of the equilibrium driving force.

Looking forward, the next step will be to extend the current analysis to model non-equilibrium conduction and Tafel plots so as to connect with more realistic electrochemical models. This work is ongoing.

ACKNOWLEDGMENTS

This material is based upon work supported by the (U.S.) Air Force Office of Scientific Research (USAFOSR) PECASE award under AFOSR Grant No. FA9950-13-1-0157.

[1] T. Holstein, Ann. Phys. **8**, 325 (1959).
[2] P. W. Anderson, Phys. Rev. **124**, 41 (1961).
[3] T. Mii, S. G. Tikhodeev, and H. Ueba, Phys. Rev. B **68**, 205406 (2003).
[4] M. Galperin, M. A. Ratner, and A. Nitzan, J. Chem. Phys. **121**, 11965 (2004).
[5] M. Galperin, M. A. Ratner, and A. Nitzan, J. Phys.: Condens. Matter **19**, 103201 (2007).
[6] A. J. White and M. Galperin, Phys. Chem. Chem. Phys. **14**, 13809 (2012).
[7] M. Thoss, I. Kondov, and H. Wang, Chem. Phys. **304**, 169 (2004).
[8] I. Kondov, M. Thoss, and H. Wang, J. Phys. Chem. A **110**, 1364 (2006).
[9] M. Thoss, I. Kondov, and H. Wang, Phys. Rev. B **76**, 153313 (2007).
[10] J. Li, I. Kondov, H. Wang, and M. Thoss, J. Phys.: Condens. Matter **27**, 134202 (2015).
[11] T. L. Schull, J. G. Kushmerick, C. H. Patterson, C. George, M. H. Moore, S. K. Pollack, and R. Shashidhar, J. Am. Chem. Soc. **125**, 3202 (2003).
[12] C. Li, D. Zhang, X. Liu, S. Han, T. Tang, C. Zhou, W. Fan, J. Koehne, J. Han, M. Meyyappan, A. M. Rawlett, D. W. Price, and J. M. Tour, Appl. Phys. Lett. **82**, 645 (2003).
[13] J. Chen, J. Su, W. Wang, and M. Reed, Phys. E **16**, 17 (2003).
[14] M. Galperin, M. A. Ratner, and A. Nitzan, Nano Lett. **5**, 125 (2005).
[15] E. Y. Wilner, H. Wang, G. Cohen, M. Thoss, and E. Rabani, Phys. Rev. B **88**, 045137 (2013).
[16] E. Y. Wilner, H. Wang, M. Thoss, and E. Rabani, Phys. Rev. B **89**, 205129 (2014).
[17] N. Bode, S. V. Kusminskiy, R. Egger, and F. von Oppen, Beilstein J. Nanotechnol. **3**, 144 (2012).
[18] B. Li, E. Y. Wilner, M. Thoss, E. Rabani, and W. H. Miller, J. Chem. Phys. **140**, 104110 (2014).
[19] W. Dou, A. Nitzan, and J. E. Subotnik, J. Chem. Phys. **142**, 084110 (2015).
[20] W. Dou, A. Nitzan, and J. E. Subotnik, J. Chem. Phys. **143**, 054103 (2015).
[21] W. Dou and J. E. Subotnik, J. Chem. Phys. **144**, 024116 (2016).

[22]W. Ouyang, W. Dou, A. Jain, and J. E. Subotnik, J. Chem. Theory Comput. **12**, 4178 (2016).
[23]N. Shenvi, S. Roy, and J. C. Tully, J. Chem. Phys. **130**, 174107 (2009).
[24]J. Mohr, W. Schmickler, and J. Badiali, Chem. Phys. **324**, 140 (2006).
[25]A. Kuznetsov, R. Nazmutdinov, and W. Schmickler, J. Electroanal. Chem. **532**, 171 (2002).
[26]A. K. Mishra and D. H. Waldeck, J. Phys. Chem. C **113**, 17904 (2009).
[27]A. K. Mishra and D. H. Waldeck, J. Phys. Chem. C **115**, 20662 (2011).
[28]W. Schmickler and J. Mohr, J. Chem. Phys. **117**, 2867 (2002).
[29]M. Thomas, T. Karzig, S. V. Kusminskiy, G. Zaránd, and F. von Oppen, Phys. Rev. B **86**, 195419 (2012).
[30]J. F. Rusling and S. L. Suib, Adv. Mater. **6**, 922 (1994).
[31]We remind the reader, however, that an inverted regime exists only in a solution, and not near a metal surface with a continuum of states.
[32]A. J. Bard and L. R. Faulkner, *Electrochemical Methods: Fundamentals and Applications*, 2nd ed. (Wiley, 2000), p. 104.
[33]W. Schmickler and E. Santos, *Interfacial Electrochemistry*, 2nd ed. (Springer, 2010), p. 94.
[34]H. Risken, *The Fokker-Planck Equation*, Methods of Solution and Applications, 2nd ed. (Springer-Verlag, 1989), p. 103.
[35]J. Cao and Y. Jung, J. Chem. Phys. **112**, 4716 (2000).
[36]W. Boucher and J. Traschen, Phys. Rev. D **37**, 3522 (1988).
[37]A. Anderson, Phys. Rev. Lett. **74**, 621 (1995).
[38]O. Prezhdo and V. Kisil, Phys. Rev. A **56**, 162 (1997).
[39]C. C. Martens and J.-Y. Fang, J. Chem. Phys. **106**, 4918 (1997).
[40]A. Donoso and C. C. Martens, J. Phys. Chem. A **102**, 4291 (1998).
[41]R. Kapral and G. Ciccotti, J. Chem. Phys. **110**, 8919 (1999).
[42]S. Nielsen, R. Kapral, and G. Ciccotti, J. Chem. Phys. **112**, 6543 (2000).
[43]D. A. Micha and B. Thorndyke, Int. J. Quantum Chem. **90**, 759 (2002).
[44]R. Balescu and W. Y. Zhang, J. Plasma Phys. **40**, 215 (1988).
[45]W. Y. Zhang and R. Balescu, J. Plasma Phys. **40**, 199 (1988).
[46]L. Zusman, Chem. Phys. **49**, 295 (1980).
[47]J. E. Straub and B. J. Berne, J. Chem. Phys. **87**, 6111 (1987).
[48]I. Rips and J. Jortner, J. Chem. Phys. **87**, 2090 (1987).
[49]J. D. Morgan and P. G. Wolynes, J. Phys. Chem. **91**, 874 (1987).
[50]Note that, in Fig. 7, we plot data from only the large coupling (4×10^{-4} a.u.) case because, for the small coupling, charge transfer is slow compared to the ramping rate so that the non-equilibrium effects are not obvious.